# A Bio-inspired and Switchable $H^+/OH^-$ Ion-channel for Room Temperature Exhaled $CO_2$ Chemiresistive Sensing

*Honghao Chen [a,b], Ruofei Lu [a,b], Yixun Gao [a b], Xiaorui Yue [a,b], Haihong Yang [c], Hao Li [a,b], Yi-Kuen Lee [d,e], Paddy J. French [f], Yao Wang [a, b] *, and Guofu Zhou [a,b]*

[a] *Guangdong Provincial Key Laboratory of Optical Information Materials and Technology & Institute of Electronic Paper Displays, South China Academy of Advanced Optoelectronics, South China Normal University, Guangzhou 510006, P. R. China.*

[b] *National Center for International Research on Green Optoelectronics, South China Normal University, Guangzhou 510006, P. R. China.*

[c] *Department of Thoracic Oncology State Key Laboratory of Respiratory Diseases, The First Affiliated Hospital of Guangzhou Medical University, Guangzhou 510006, P.R. China*

[d] *Department of Mechanical & Aerospace Engineering, Hong Kong University of Science and Technology, Clear Water Bay, Kowloon, Hong Kong Special Administrative Region*

[e] *Department of Electronic & Computer Engineering, Hong Kong University of Science and Technology, Clear Water Bay, Kowloon, Hong Kong Special Administrative Region*

[f] *BE Lab, Faculty EWI, Delft University of Technology, Delft 2628CD, The Netherland*

** Corresponding author: Yao Wang*

*E-mail addresses: wangyao@m.scnu.edu.cn*

# Table of contents

## 1. Supplement to the characterization of materials

The weak absorption peaks around 1593 $cm^{-1}$ of the FTIR plot are attributed to the $COO^-$ asymmetric stretching vibration of RhB, TMRM and respectively. The weak absorption peaks around 1695 $cm^{-1}$ and 1710 $cm^{-1}$ of the FTIR plot are attributed to the C=O and C=N stretching vibration of RhB or TMRM respectively.[40]

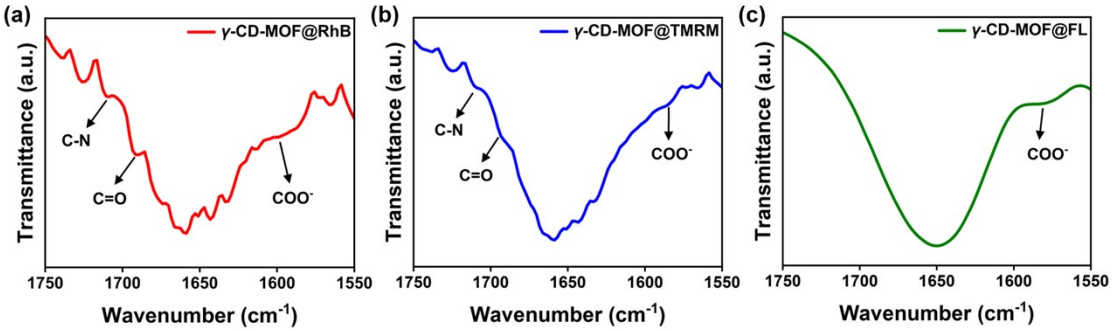


**Fig. S1** FTIR plot of (a) γ-CD-MOF@RhB, (b) γ-CD-MOF@TMRM and (c) γ-CD-MOF@FL with abscissa between 1750-1550 $cm^{-1}$.

The K 2p spectrum of the γ-CD-MOF, γ-CD-MOF@RhB, γ-CD-MOF@TMRM and γ-CD-MOF@FL shows K-O bonds at around 293 eV (Fig. S2), indicating that $K^+$ forms a coordination bond with the hydroxyl group of cyclodextrin.

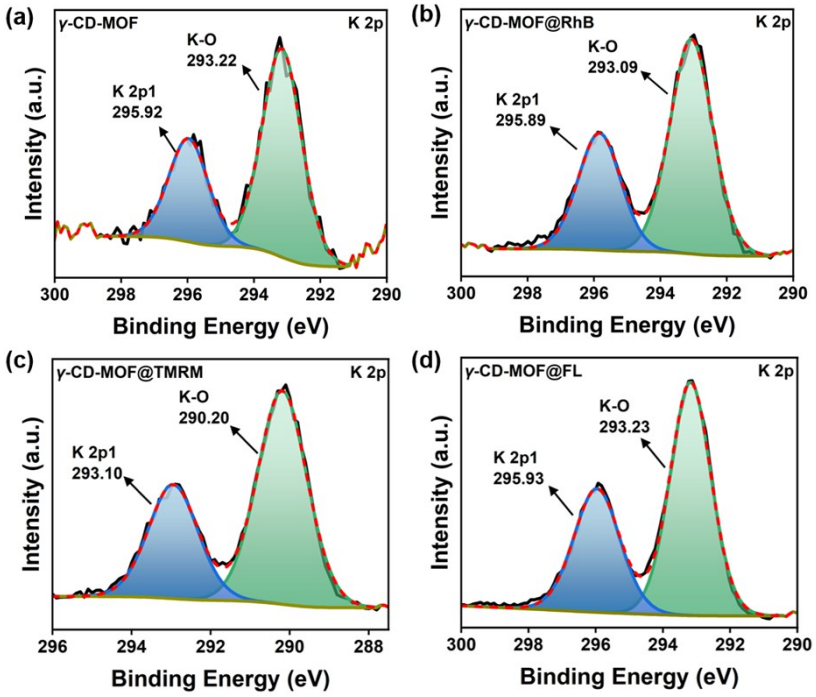


**Fig. S2** XPS spectrum of (a-d) K 2p of the γ-CD-MOF, γ-CD-MOF@RhB, γ-CD-MOF@TMRM and γ-CD-MOF@FL.

The C 1s spectrum of γ-CD-MOF@TMRM shows C-C/C=C, C-N, C-O (epoxy carbon) and C=O bonds at 284.80, 285.74, 287.35 and 288.95 eV (Fig. S3b), while its N 1s and O 1s spectrum shows the existence of C-N, C=N, C=O and C-O bonds at 398.89, 399.92, 531.33, 533.53 eV (Fig. S3a, c).

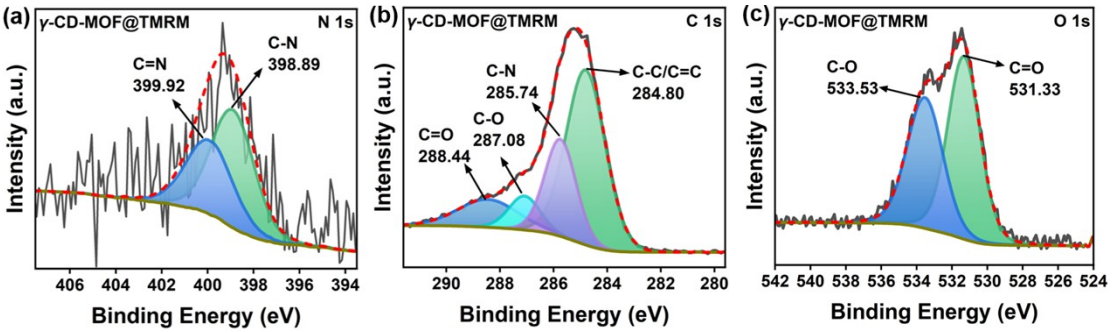


**Fig. S3** XPS spectrum of (a-c) N 1s, C 1s, O 1s of the γ-CD-MOF@TMRM.

The C 1s spectrum of γ-CD-MOF@FL shows C-C/C=C, C-O (epoxy carbon) and C=O bonds at 284.80, 286.60 and 288.50 eV (Fig. S4a), while its O 1s spectrum shows the existence of C=O and C-O bonds at 531.20, 533.40 eV (Fig. S4b).

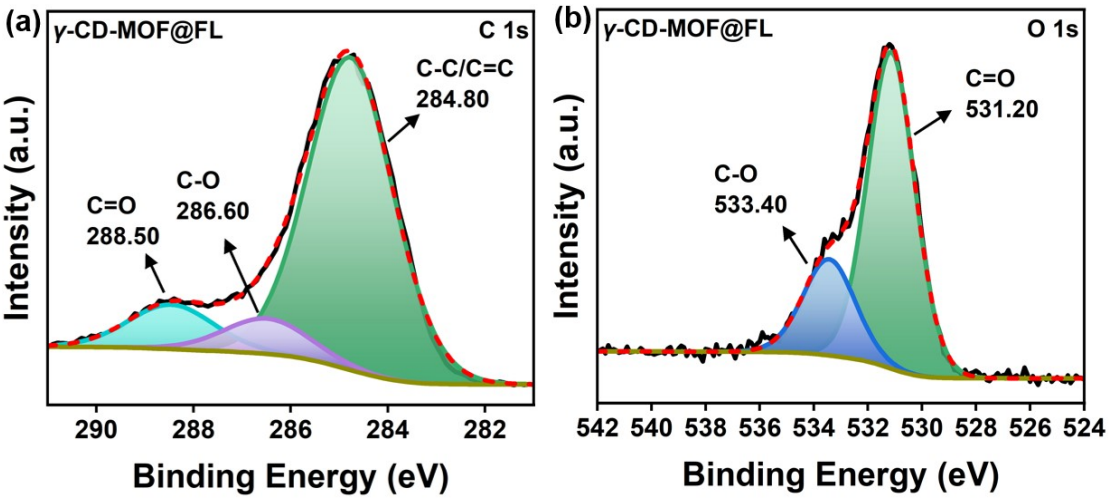


**Fig. S4** XPS spectrum of (a-b) C 1s and O 1s of the γ-CD-MOF@FL.

In order to illustrate the porosity of the material, nitrogen adsorption-desorption isotherms and pore size distributions of γ-CD-MOF and γ-CD-MOF@RhB were tested, and the results illustrate the microporous structures of γ-CD-MOF and γ-CD-MOF@RhB.

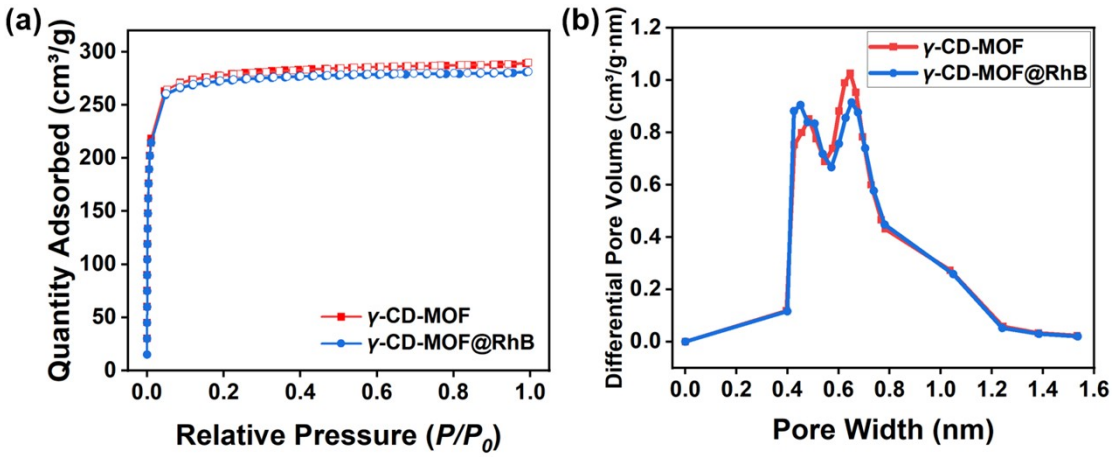


Fig. S5 (a) Nitrogen adsorption-desorption isotherms of γ-CD-MOF@RhB and γ-CD-MOF. (b) Pore size distribution of γ-CD-MOF@RhB and γ-CD-MOF.

## 2. Fluorescence spectrophotometer measurement details

To verify that fluorescein (FL) was successfully encapsulated into the γ-CD-MOF, fluorescence spectra were measured. As shown in Fig. S6, FL was successfully encapsulated into γ-CD-MOF (excitation wavelength at 478 nm and emission wavelength at 516 nm).

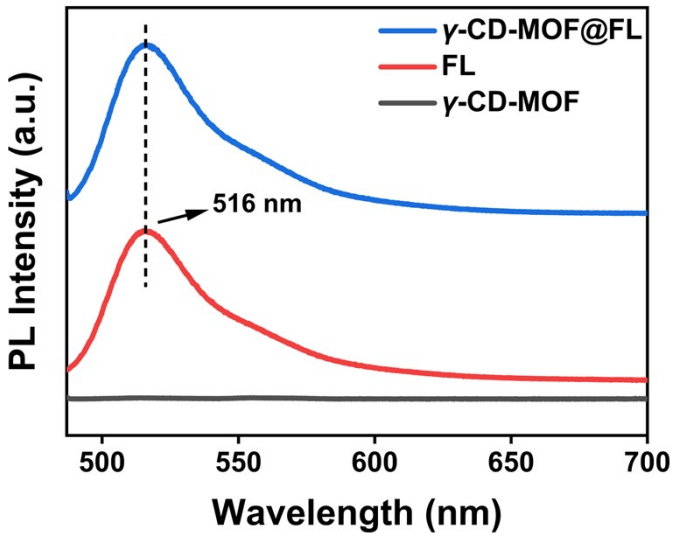


**Fig. S6** Fluorescence curve of γ-CD-MOF, FL and γ-CD-MOF@FL.

Owing to verify the actual load of fluorophores in γ-CD-MOF, the fluorescence curves and calibration curves of RhB are shown in Fig. S7a-e. Subsequently, the fluorescence curves of composite with different feeding ratios are shown in Fig. S7f,

which can estimate the actual load of RhB in γ-CD-MOF according to the calibration curve (Table S1).

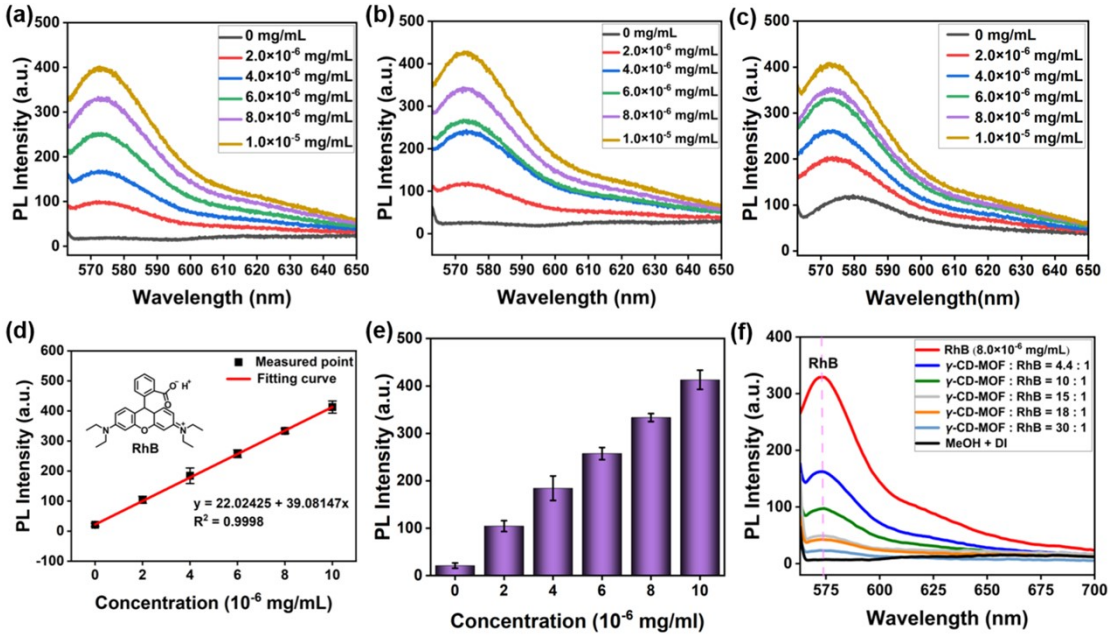


**Fig. S7** (a-c) Fluorescence curve of RhB. (d-e) RhB calibration curve drawn according to fluorescence curve. (f) Fluorescence curves of γ-CD-MOF@RhB with different feed ratios

The fluorescence curves and calibration curves of TMRM are shown in Fig. S8a-d. The fluorescence curves of composite with different feeding ratios are shown in Fig. S8e, the actual load of TMRM in γ-CD-MOF are shown in Table S1.

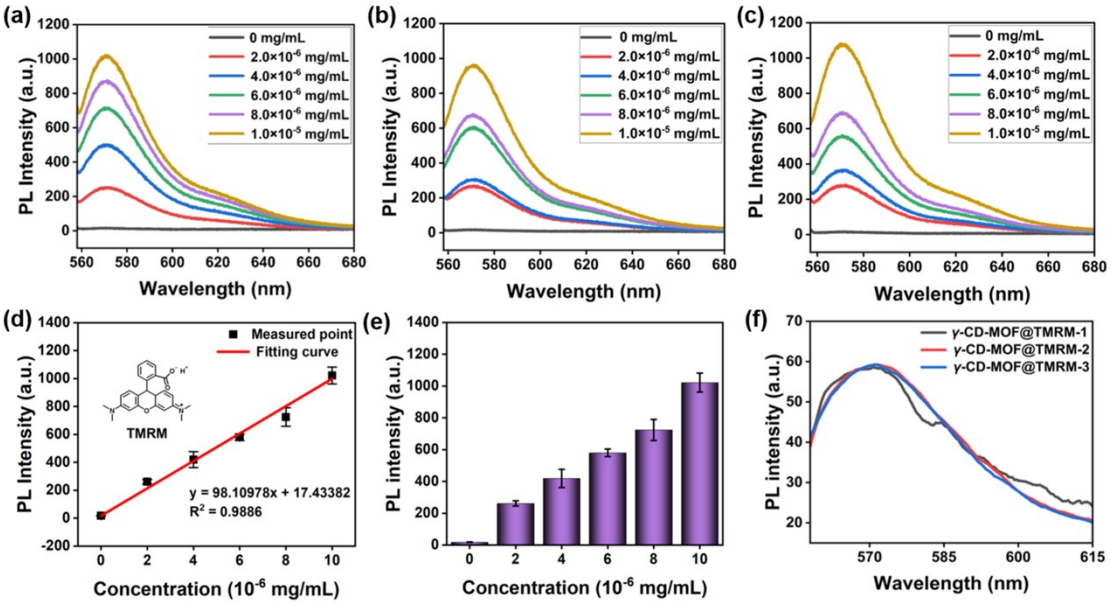


**Fig. S8** (a-c) Fluorescence curve of TMRM. (d-e) TMRM calibration curve drawn according to fluorescence curve. (f) Fluorescence curves of γ-CD-MOF@TMRM.

The fluorescence curves and calibration curves of FL are shown in Fig. S9a-d. The fluorescence curves of composite with different feeding ratios are shown in Fig. S9e, the actual load of FL in γ-CD-MOF are shown in Table S1.

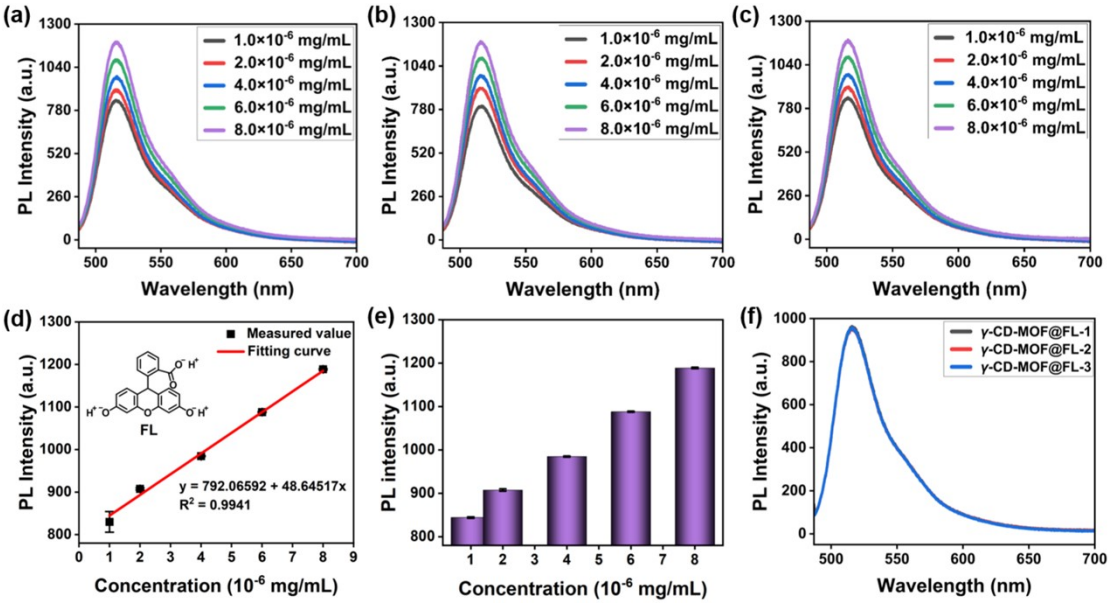


**Fig. S9** (a-c) Fluorescence curve of FL. (d-e) FL calibration curve drawn according to fluorescence curve. (f) Fluorescence curves of γ-CD-MOF@FL.

**Table S1.** The feeding ratio of γ-CD to fluorophore and the estimated molar ratio of γ-CD-MOF to fluorophore based on the fluorescence calibration curve.

| feed ratio γ-CD: RhB | mole ratio γ-CD-MOF: RhB | feed ratio γ-CD: TMRM | mole ratio γ-CD-MOF: TMRM | feed ratio γ-CD: FL | mole ratio γ-CD-MOF: FL |
|---|---|---|---|---|---|
| **30: 1** | **26.85: 1** | **/** | **/** | **40: 1** | **26.98: 1** |
| **18: 1** | **11.39: 1** | **1: 1** | **11.32: 1** | **/** | **/** |
| **15: 1** | **6.68: 1** | **/** | **/** | **/** | **/** |
| **10: 1** | **2.25: 1** | **/** | **/** | **/** | **/** |
| **4.4: 1** | **1.17: 1** | **/** | **/** | **/** | **/** |

## 3. Response recovery curve of γ-CD-MOF@RhB toward 1000 ppm $CO_2$ at different humidity and pH measurement

Owing to explore the effect of humidity, the sensor was placed at a relative humidity of 5-70 % (RH) and then the response of 1000 ppm $CO_2$ was measured. The results show that the response value decreases with increasing humidity, which is attributed to the competition between $H_2O$ and $CO_2$ adsorbed on the surface of the material. This problem can be solved by drying the target gas in advance.

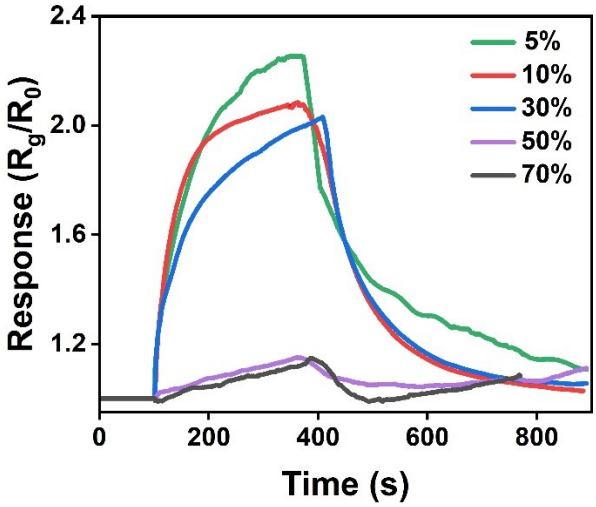


**Fig. S10** The gas sensing responses of γ-CD-MOF@RhB toward 1000 ppm of $CO_2$ under 5–70% relative humidity.

To confirm the dominant type of ion-conduction, the pH of the γ-CD-MOF@RhB dispersion was measured. The results showed that the dispersion of γ-CD-MOF@RhB was alkaline.

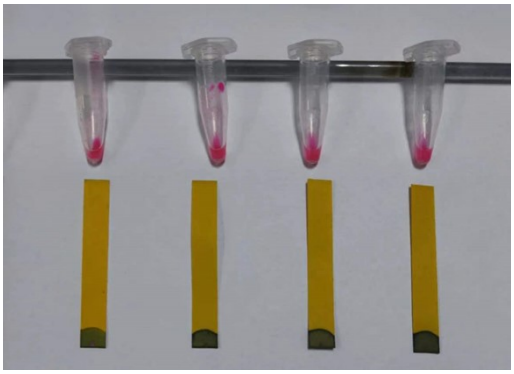

**Fig. S11** pH measurement of dispersion of γ-CD-MOF@RhB.

## 4. Comparison with commercial IR carbon dioxide meter

As shown in Fig. S12, the commercial carbon dioxide meter is put into a 5 L sealed test chamber and calibrated in the test environment to obtain an initial value. Then inject different concentrations of $CO_2$, and the difference between the reading of the concentration value after the response is stable and the initial value is the response value (Table S2).

In addition, a comparison video of sensing with commercial IR $CO_2$ meters (Vedio-1) and real-time detection video of the chemiresistive $CO_2$ sensor (Vedio-2) were provided in the supporting information.

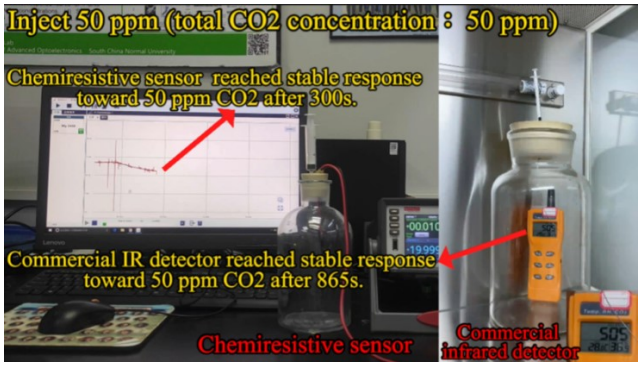


**Fig. S12** Comparison of real-time response between commercial IR carbon dioxide meter and our sensor toward 50 ppm $CO_2$.

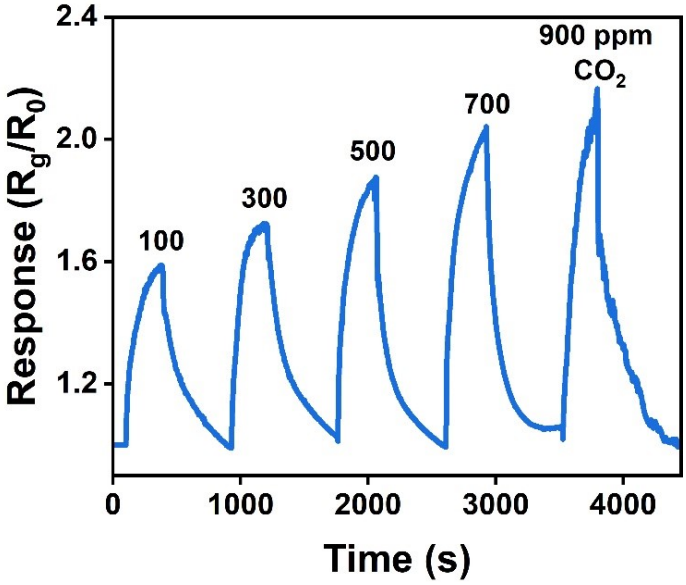


**Fig. S13** Sensing performance of our sensor toward 100-900 ppm $CO_2$.

**Table S2.** Comparison of $CO_2$ concentration detected by our sensor and commercial IR $CO_2$ meter.

| Value of actual injected $CO_2$ (ppm) | Our sensor (ppm) | commercial IR meter (ppm) | Response time of our sensor (s) | Response time of commercial $CO_2$ meter (s) |
|---|---|---|---|---|
| **100** | **127** | **144** | **178** | **960** |
| **300** | **341** | **338** | **132** | **780** |
| **500** | **531** | **547** | **181** | **840** |
| **700** | **721** | **744** | **221** | **840** |
| **900** | **924** | **947** | **220** | **1080** |

## 5. Real-time detection and exhaled breath detection equipment

To further demonstrate the potential of the sensor for practical applications, real-time detection experiments were conducted on the sensor (Fig. S14). In order to avoid the influence of humidity in the exhaled breath, the exhaled breath was collected into a 1 L gas collection bag and then tested using a syringe to take a certain amount of exhaled breath via a drying device (Fig. S15). In addition, Table 3 shows the information of volunteers. The exhaled breath used in this study comes from volunteers in our research group and does not reveal personal information or involve any medical ethics.

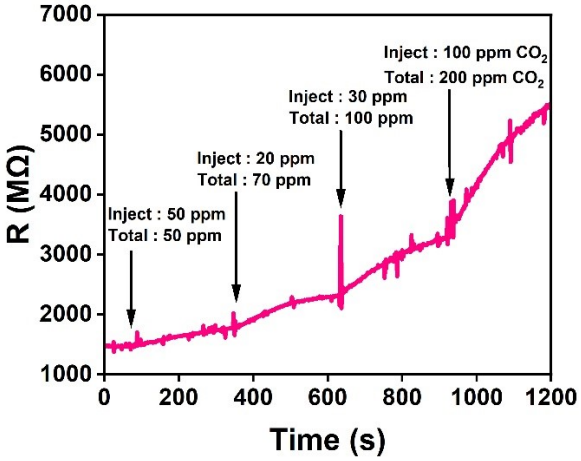


**Fig. S14** Real-time response curve of resistance toward 50-200 ppm $CO_2$.

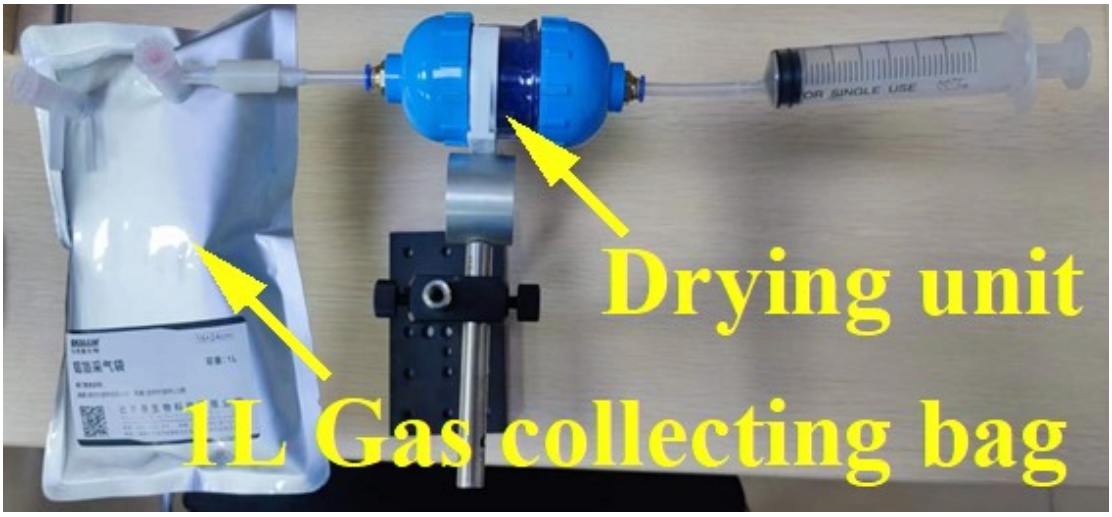


**Fig. S15** Schematic diagram of the simple drying unit.

**Table S3.** Information of volunteers.

| Individual Classification | No. | Gender | Age | Time from recovery day to breath test day * | Pulmonary function assessment |
|---|---|---|---|---|---|
| Undiseased | 1 | female | 27 | / | Normal |
| | 2 | male | 25 | / | Normal |
| | 3 | male | 23 | / | Normal |
| | 4 | male | 28 | / | Normal |
| | 5 | male | 24 | / | Normal |
| COVID-19 rehabilitative volunteers | 6 | female | 23 | 2 days | Abnormal |
| | 7 | male | 24 | 3 days | Abnormal |
| | 8 | male | 28 | 2 days | Abnormal |
| | 9 | male | 25 | 3 days | Normal |
| | 10 | male | 26 | 3 days | Normal |

* Recovery day is defined as the day when COVID-19 rehabilitative volunteers' antigen test shows negative.

The gas collection process can be completed in 10 ± 5 s, and the total time from the start of gas collection to the completion of the gas test is about 800 ± 147 s.

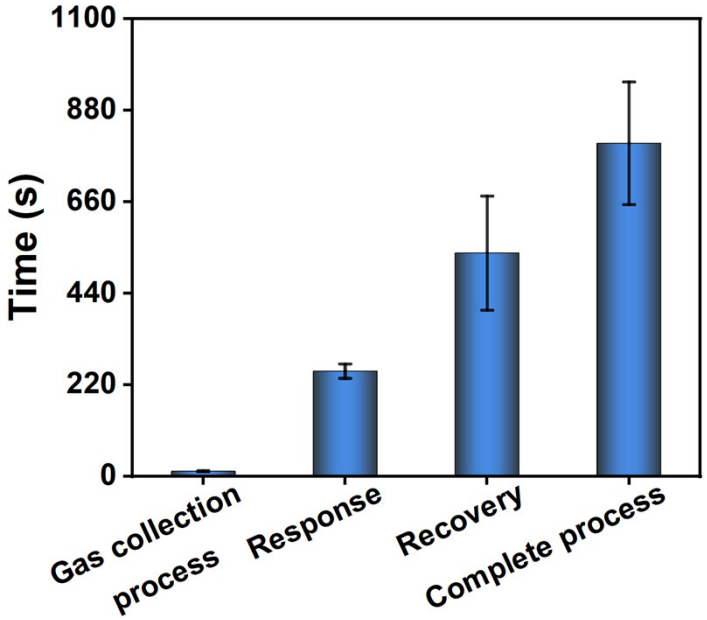


Fig. S16. Gas collection process (Including drying, extraction and injection), response, recovery and complete process times for human breath testing.

## 6. Estimation of proton conductivity ($\sigma$) and activation energy ($E_a$).

Calculate the proton conductivity ($\sigma$) of the material by the following equation，

$$\sigma = \frac{l}{RA}$$

where $R$ is the sheet resistance estimated based on EIS data, $l$ is the thickness of the sheet, and $A$ is the cross-sectional area of the sheet. The converted conductivity value is shown in Table S3.

Arrhenius equation is used to estimate the activation energy ($E_a$) of proton conduction of materials,

$$\ln(\sigma T) = \ln(\sigma_0) - \frac{E_a}{K_B T}$$

where $\sigma_0$ is the pre-exponential factor, T is the temperature, $k_B$ is the Boltzmann constant, which is $8.617 \times 10^{-5}$ eV/K. Draw the relationship plot of ln($\sigma$T) to (1000/T), and determine the $E_a$ value of the material according to the slope of the plot (Fig. 7f).